Synthetic auxotrophy remains stable after continuous evolution and in co-culture with mammalian cells

Authors: Aditya M. Kunjapur[1,2†]*, Michael G. Napolitano[1,3†], Eriona Hysolli[1†], Karen Noguera[1], Evan M. Appleton[1], Max G. Schubert[1], Michaela A. Jones[2], Siddharth Iyer[4], Daniel J. Mandell[1,5] & George M. Church[1]*

Affiliations:

[1]Department of Genetics, Harvard Medical School, 77 Avenue Louis Pasteur, NRB 238, Boston, MA 02115, USA.

[2]Present Address: Department of Chemical and Biomolecular Engineering, University of Delaware, 150 Academy Street, CLB 215, Newark, DE 19716, USA

[3]Present Address: Ginkgo Bioworks, 27 Drydock Avenue, 8th Floor, Boston, MA 02210, USA.

[4]Present Address: Johns Hopkins University, 3101 Wyman Park Drive, Baltimore, MD 21218, USA

[5]Present Address: GRO Biosciences, 700 Main Street North, Cambridge, MA 02139, USA.

*Corresponding authors: AMK (kunjapur@udel.edu) or GMC (gchurch@genetics.med.harvard.edu).

†These authors contributed equally to this work.

Abstract:

Understanding the evolutionary stability and possible context-dependence of biological containment techniques is critical as engineered microbes are increasingly under consideration for applications beyond biomanufacturing. While synthetic auxotrophy previously prevented *Escherichia coli* from exhibiting detectable escape from batch cultures, its long-term effectiveness is unknown. Here, we report automated continuous evolution of a synthetic auxotroph while supplying a decreasing concentration of essential biphenylalanine (BipA). After 100 days of evolution, triplicate populations exhibit no observable escape and exhibit normal growth rates at 10-fold lower BipA concentration than the ancestral synthetic auxotroph. Allelic reconstruction reveals the contribution of three genes to increased fitness at low BipA concentrations. Based on its evolutionary stability, we introduce the progenitor strain directly to mammalian cell culture and

observe containment of bacteria without detrimental effects on HEK293T cells. Overall, our findings reveal that synthetic auxotrophy is effective on timescales and in contexts that enable diverse applications.

One Sentence Summary:

Continuous evolution of a synthetic auxotrophic *Escherichia coli* strain does not lead to observable escape from biocontainment, demonstrating that life does not always find a way.

Main Text:

Introduction

New safeguards are needed for the deliberate release of engineered microbes into the environment, which has promise for applications in agriculture, environmental remediation, and medicine (*1*). Genetically encoded biocontainment strategies enable attenuation of engineered live bacteria for diverse biomedical applications(*2–4*), including as potential vaccines (*5–10*), diagnostics (*11*), and therapeutics (*12–15*). Auxotrophy, which is the inability of an organism to synthesize a compound needed for its growth, is an existing strategy for containment. However, foundational studies of auxotrophic pathogens demonstrated proliferation in relevant biological fluids (*16*) and reversion to prototrophy upon serial passaging (*17*, *18*). Modern genome engineering strategies can prevent auxotrophic reversion, and auxotrophy has been a key component of microbial therapies that have reached advanced clinical trials. However, the ability for auxotrophs to access required metabolites within many host microenvironments, and after leaving the host, remains unaddressed. Auxotrophy may not be effective in scenarios where engineered living bacteria encounter metabolites from dead host cells (*19*) or invade host cells (*20*). Indeed, growth of double auxotrophs is supported *in vivo* by neoplastic tissue (*13*). Auxotrophy may also be insufficient for tight control of cell proliferation in environments rich with microbial sources of cross-feeding (*21*), such as gut, oral, skin, and vaginal microbiomes. Given that most naturally occurring microorganisms are auxotrophs (*22*), it is also unlikely that auxotrophy will limit the spread of an engineered microbe once it leaves the body and enters the environment.

Synthetic auxotrophy may overcome these hurdles by requiring provision of a synthetic molecule for survival of the engineered bacteria. This strategy was first implemented successfully in *E. coli* by engineering an essential protein to depend on incorporation of a non-standard amino acid (nsAA) (*23*, *24*). We previously engineered *E. coli* strains for dependence on the nsAA biphenylalanine (BipA) by computer-aided redesign of essential enzymes in conjunction with expression of orthogonal translation machinery for BipA incorporation (*23*). Among several synthetic auxotrophs originally constructed, one strain harbored three redesigned, nsAA-dependent genes: Adenylate kinase (*adk.d6*), tyrosyl-tRNA synthetase (*tyrS.d8*), and BipA-dependent aminoacyl-tRNA synthetase, for aminoacylation of BipA (*BipARS.d6*). This BipA-dependent strain, dubbed "DEP", exhibited undetectable escape throughout 14 days of monitoring

at an assay detection limit of $2.2x10^{-12}$ escapees per colony forming unit (CFU) (*23*). Though this strain demonstrates effective biocontainment in 1 L batch experiments, its precise escape frequency and long-term stability remained unexplored.

Here, we perform the first study of evolutionary stability of a synthetic auxotroph, with the aid of automated continuous evolution. Continuous evolution better emulates scenarios where biocontainment may be needed by fostering greater genetic variability within a population. We posited that decreasing BipA concentrations would add selective pressure for adaptation or for escape, either of which would be enlightening. Adaptive laboratory evolution of DEP may improve its fitness in relevant growth contexts, as previously demonstrated for its non-auxotrophic but recoded ancestor, C321.ΔA (*25*). We report that DEP maintains its inability to grow in the absence of synthetic nutrient, even after three parallel 100-day chemostat trials. Additionally, we find evidence of adaptation, with evolved DEP isolates requiring 10-fold lower BipA concentration to achieve optimal growth than ancestral DEP (0.5 μM rather than 5 μM). We resequence evolved populations and perform allelic reconstruction in ancestral DEP using multiplex automatable genome engineering (MAGE), identifying alleles that partially restore the adaptive phenotype. Finally, we advance this technology towards host-microbe co-culture applications, demonstrating direct mixed culture of DEP and mammalian cells without need for physical barriers nor complex fluidics.

Results and Discussion

To perform continuous evolution of *E. coli*, we constructed custom chemostats for parallelized and automated culturing (**Fig. 1A**). Our design and construction was based on the eVOLVER system (*26*), an open-source, do-it-yourself automated culturing platform (**Figs. S1-S4**). By decreasing BipA concentration over time in our chemostats, we provide an initial mild selection for escape and steadily increase its stringency. This design is analogous to a "morbidostat", where a lethal drug is introduced dynamically at sub-lethal concentrations to study microbial drug resistance (*27*), but with synthetic auxotrophy providing selective pressure. Our working algorithm for automated adjustment of BipA concentration as a function of turbidity is shown in **Fig. 1B**, and a representative image of our hardware is shown in **Fig. 1C** (see also **Fig. S5**).

Our long-term culturing experiments featured two phases. The first phase included one chemostat (N=1) that was inoculated with DEP for an 11-day incubation, with an initial concentration of BipA of 100 μM and automated adjustment based on growth rate (**Fig. 2A**). Because we observed no colony formation when the outgrowth from this population was plated on non-permissive media, we then began a second phase in replicate. We used our population grown for 11 days to inoculate three chemostats in parallel (N=3) where BipA supply decreased automatically over the following 90 days from 100 μM to nearly 100 nM. One controller provided identical BipA concentrations to all 3 vials at any given time. To determine whether the decrease in BipA supply was due to escape from dependence on BipA, we periodically performed escape assays. We continued to observe no escape, including when we seeded liter-scale cultures and plated the associated outgrowth on non-permissive media. Evolved isolates were obtained after this procedure (**Fig. S6**), and their growth was characterized across BipA concentrations (**Fig. 2B and S7**). At 0.5-1 μM BipA, we observed growth of all evolved isolates, and no growth of the ancestral DEP strain.

To identify the causal alleles contributing to decreased BipA requirement of all three evolved isolates, we performed whole-genome sequencing and mutational analysis. We expected that mutations in auxotrophic markers or orthogonal translation machinery associated with aminoacylation of BipA would be observed. However, no variants were detected in the plasmid-expressed orthogonal translation machinery (aminoacyl-tRNA synthetase and tRNA) reference sequence. Instead, in all three evolved isolates, variants were observed in three non-essential genes, all of which are implicated in molecular transport: *acrB*, *emrD*, and *trkH* (**Fig. 3A**). AcrB and EmrD are biochemically and structurally well-characterized multi-drug efflux proteins (*28*), and TrkH is a potassium ion transporter (*29*). These exact mutations have no precedent in the literature to our knowledge. Because they are missense mutations or in-frame deletions, it is unclear whether they cause loss of function or altered function (**Table S1**). Because permissive media contains four artificial targets of efflux (BipA, L-arabinose, chloramphenicol, and SDS), mutations that confer a selective advantage during continuous evolution could disable BipA/L-arabinose efflux, improve chloramphenicol/SDS efflux, or affect transport of these or other species more indirectly. Given the strong selective pressure enforced by decreasing BipA concentration, we hypothesize that mutations observed are more likely to affect BipA transport. We also observed mutations in all evolved populations to the 23S ribosomal RNA (rRNA) gene *rrlA* (**Table S2**). 23S rRNA

mutations have been found to enhance tolerance for D-amino acids (*30*) and β-amino acids (*31*). However, 23S rRNA mutations could also be related to increased tolerance of chloramphenicol (*32*).

To learn how identified transporter alleles may contribute to increased growth rates at low BipA concentration, we performed allelic reconstruction in the progenitor DEP strain using multiplexed automatable genome engineering (MAGE) (*33*). Among four mutants that we generated in DEP, we observed growth of all mutants at 2 μM BipA, a condition in which progenitor DEP could not grow (**Fig. 3B and S8**). Furthermore, only *emrD* mutants exhibited near-normal growth at 1 μM BipA. To investigate possible differential sensitivity of strains that contain reconstructed alleles to other media components of interest (SDS, L-arabinose, Tris buffer, and Chloramphenicol), we varied the concentration of these components and measured doubling times (**Fig. S9**). We observed no significant deviation in doubling time from DEP in any of these cases. These results collectively suggest that observed transporter alleles are linked to BipA utilization.

The unobservable escape of DEP even after 100 days of evolution encouraged us to explore the possibility of an improved *in vitro* model for host-microbe interactions. *In vitro* models allow direct visualization and measurement of cells and effectors during processes such as pathogenesis (*34*). They are more relevant than animal studies for several human cell-specific interactions due to biological differences across animal types (*35*, *36*). A non-pathogenic *E. coli* strain engineered to express heterologous proteins could be particularly useful for studying or identifying virulence factors and disease progression. However, an obstacle associated with co-culture of microbial and mammalian cells is microbial takeover of the population. Approaches used to address this are bacteriostatic antibiotics (*37*), semi-permeable Transwell membranes (*38–40*), microcarrier beads (*41*), microfluidic cell-trapping (*42*), peristaltic microfluidic flow (*43*, *44*), and microfluidic perfusion (*45*). However, the use of a well-characterized synthetic auxotroph capable of limited persistence could offer a superior alternative for spatiotemporal control of microbial growth, especially for studying longer duration phenomena such as chronic infection or wound healing. Our study demonstrates how temporal control can be achieved by removal of BipA; we anticipate that spatial control could be achieved by patterning BipA onto a variety of solid surfaces with limited diffusion, such as a skin patch.

We investigated mammalian cell culture health, growth, and morphology after simple transient exposure to a hypermutator variant of DEP that we engineered by inactivating *mutS*

during allelic reconstruction (DEP*). The use of DEP* rather than DEP is yet another form of a stress test to increase opportunity for escape under co-culture conditions. We directly co-cultured adherent human cell line HEK293T with either no bacteria, non-auxotrophic *E. coli* DH5α, or DEP* overnight (24 hours). HEK293T cells were cultured in selection media that allow only growth of desired but not contaminant strains while selecting for bacterial plasmid maintenance. After co-culture, we washed cells, and replenished cells with media varying in inclusion of BipA and/or an antibiotic cocktail (Penicillin/Streptomycin/Amphotericin B). We continued incubation and imaged cells at Days 2, 4, and 7 after initial co-incubation. HEK293T cells contain a copy of mCherry integrated into the AAVS1 locus and they appear red. DH5α and DEP* were transformed with Clover green fluorescent protein prior to co-culture and appear green.

Compared to the control culture where bacteria were not added (**Fig. 4A**), HEK293T cells co-cultured with DH5α display visible bacterial lawns with no attached human cells in the absence of the antibiotic cocktail at all days of observation (**Fig. 4B**). In the presence of antibiotic, co-cultures containing DH5α sharply transition from bacterial overgrowth to apparent bacterial elimination (**Fig. 4C**). In contrast, cells co-cultured with DEP* in the absence of BipA exhibited similar morphology to the control at all days of observation and no detectable bacteria by fluorescence microscopy on Day 7, without the need for antibiotics to achieve bacterial clearance (**Fig. 4D**). Thus, DEP* addition was not detrimental to HEK293T cells in the absence of BipA and DEP* remains biocontained and cannot survive because of cross-feeding. Clearance of bacterial cells from human cells appears to occur faster for DEP* when not provided BipA (**Fig. 4D**) than for DH5α when provided the antibiotic cocktail (**Fig 4C**).

To learn how the synthetic auxotroph behaves when supplied its essential nutrient in these co-culture settings, we tested DEP* co-cultures with continual resupply of 100 μM BipA. Here, DEP* proliferates and in turn decreases proliferation and viability of HEK293T cells (**Fig. 4E**). A bacterial lawn begins to form on Day 2 and at later times human cell debris is overtaken by DEP*. This demonstrates that DEP* is fully capable of taking over the co-culture if supplied with BipA. Replicates for these experiments can be found in **Figs. S10-12**.

Given that DEP* grows in co-cultures when BipA is provided, we sought to understand whether it could be rescued by re-addition of BipA after multiple days of withholding. The possible timescale of re-emergence influences applications where the duration of bacterial activity would need to be prolonged and/or repeated via limited BipA introduction while remaining contained.

We find that co-culturing DEP* with HEK293T cells for 2 days in absence of BipA followed by addition of BipA at Day 2 does not rescue the DEP* growth (**Fig. 4F and S13**). Human cells still grow and look morphologically similar to untreated cells and bacteria are not visible. To look at analogous questions for non-auxotrophic *E. coli*, we removed antibiotics after 2 days of co-culturing and do not observe bacterial rescue (**Fig. S13)**. We also investigated whether bacterial clearance could be delayed by addition of antibiotic after some growth of DH5α. DH5α cells grown in absence of the antibiotic cocktail for 2 days before addition of the cocktail and maintenance to Day 7 result in bacterial lawns (**Fig. S13A/D**). This demonstrates that antibiotic cocktails ordinarily used in mammalian cell culture maintenance can become ineffective beyond a certain amount of non-auxotrophic bacterial growth, whereas synthetic auxotrophy is subject to fewer and different constraints.

To further investigate the persistence of progenitor DEP and its evolved descendants, we performed BipA re-addition studies in LB monoculture. Within 7 hours of BipA removal, DEP cell populations that are harvested from mid-exponential or stationary phases can be "reactivated" upon delayed BipA addition with unperturbed growth kinetics after a highly tunable lag phase (**Fig. S14)**. Further studies are ongoing to investigate the amount of time after which BipA reintroduction can recover growth of synthetic auxotrophs under different contexts.

We have shown that synthetic auxotrophy can exhibit long-term stability and function in unique contexts, enabling reliable control of microbial proliferation. Recent work has also shown that the escape rate and fitness of multiple synthetic auxotrophs can be improved by increasing the specificity of nsAA incorporation machinery (*46*). Collectively, these engineering and characterization efforts advance synthetic auxotrophy as a powerful safeguard for basic and applied research when using engineered microbes.

Materials and Methods

Culture conditions

Cultures for general culturing, growth rate assays, biocontainment escape assays, MAGE, and fluorescent protein assays were prepared in LB-Lennox medium (LB^L: 10 g/L bacto tryptone, 5 g/L sodium chloride, 5 g/L yeast extract) supplemented with 15 μg/mL chloramphenicol, 0.2% (wt/v) L-arabinose, 20 mM Tris-HCl buffer, 0.005% SDS, and variable concentration of *L*-4,4-Biphenylalanine (BipA). Unless otherwise indicated, all cultures were grown in 96-well deep plates in 300 μL culture volumes at 34 °C and 400 rpm. The above media is permissive for growth of the synthetic auxotroph. Non-permissive media is identically formulated as permissive media except for BipA, which is not included.

Construction of custom chemostats

Construction of appropriate fluidics and chambers followed the eVOLVER framework (*26*) (**Figs. S1 and S2)**. The following components were included: (1) Fluidics and chambers (reactor vial, inlet and outlet lines, filters, pumps, stirrers, and inlet and outlet reservoirs); (2) Light source and detector (LED and photodiode); (3) Controller hardware (circuit and microprocessors); (4) Controller software (Arduino for controlling tasks, Raspberry Pi for computing tasks, Python code for programming tasks) (full Build of Materials included in **Table S3**). Briefly, our apparatus consisted of a custom "smart sleeve" (**Fig. S3**), with the following modifications: Each vial was constructed without temperature control and was supplied by two media pumps (one for permissive media, another for non-permissive media) and connected to one waste pump. All pumps were RP-Q1 from Takasago fluidics, each driven off a standard N power MOSFET with an Arduino controlling the gate. Like the eVOLVER system, we installed a stirring fan underneath each sleeve that consisted of magnets attached to a computer fan. By including a small stir bar within each reactor vial, we enabled efficient mixing of 1 mL working volumes. To enable automated measurement of turbidity (optical density, or OD), we used a 605 nm LED (LO Q976-PS-25) and an OPT101P-J photodiode detector. We mounted the LED and detector on custom PCBs mounted to the vial sleeve to enable easier construction and better control of ambient light leakage into the light path (**Fig. S4**). To monitor turbidity within each vial and to control pump arrays in response, we constructed printed circuit board designs in Gerber format as is standard for circuit fabrication. We attached an Arduino Mega microcontroller with an Analog-Digital Converter and directed it using a PyMata script (*47*).

Operation of custom chemostats

Chemostats were operated by automated maintenance of culture OD within a specified parameter range within exponential growth phase (20-80% of dynamic range) depending on linearity of photodiode measurements. Constant fixed dilutions of permissive media were used to decrease OD until desired equilibrium of cell growth and dilution rates. This resulted in a sawtooth curve (*27*), where time between peaks is recorded as a proxy for growth rate. Our program gradually decreased the ratio of permissive to non-permissive media as step functions, with a specified number of dilution cycles allowed to elapse before the next decrease to provide time for acclimation. Time between OD peaks lengthened as strain fitness decreased. Once a threshold difference between ancestral peak-to-peak time and current peak-to-peak time was passed, the ratio of permissive to non-permissive media remained fixed. This allowed cells to evolve until peak-to-peak time returns to ancestral values, which initiated the next phase of decrease in BipA concentration. To assess the quality of our continuous evolution process, we paused chemostat trials on a weekly basis for strain storage, strain evaluation, chemostat cleaning, and investigation of contamination.

Measurement of doubling times

Growth assays were performed by plate reader with blanking as previously described (*48*). Overnight cultures were supplemented with different BipA concentrations depending on the strain. The DEP progenitor strain was grown in permissive media containing 100 μM BipA, and evolved DEP strains DEP.e3, DEP.e4, and DEP.e5 were grown in permissive media containing 1 μM BipA. Saturated overnight cultures were washed twice in LB and resuspended in LB. Resuspended cultures were diluted 100-fold into three 150 μL volumes of permissive media. BipA concentrations used in this assay were: 0 μM, 0.001 μM, 0.01 μM, 0.1 μM, 0.5 μM, 1 μM, 10 μM,

and 100 μM. Cultures were incubated in a flat-bottom 96-well plate (34 °C, 300 r.p.m.). Kinetic growth (OD_{600}) was monitored in a Biotek Eon H1 microplate spectrophotometer reader at 5-min intervals for 48 h. The doubling times across technical replicates were calculated as previously indicated. We refer to these as technical replicates because although triplicate overnight cultures were used to seed triplicate experiment cultures, the overnight cultures were most often seeded from one glycerol stock.

Escape frequency assays

Escape assays were performed as previously described with minor adjustments to decrease the lower detection limit for final evolved populations (*46, 49*). Strains were grown in permissive media and harvested in late exponential phase. Cells were washed twice with LB and resuspended in LB. Viable CFU were calculated from the mean and standard error of the mean (SEM) of three technical replicates of tenfold serial dilutions on permissive media. Twelve technical replicates were plated on noble agar combined with non-permissive media in 500 cm^2 BioAssay Dishes (Thermo Scientific 240835) and monitored daily for 4 days. If synthetic auxotrophs exhibited escape frequencies above the detection limit (lawns) on non-permissive media, escape frequencies were calculated from additional platings at lower density. The SEM across technical replicates of the cumulative escape frequency was calculated as previously indicated.

Genome resequencing and analysis

Genomic DNA was obtained from evolved populations and ancestral clone using the Wizard Genomic DNA purification kit (Promega). Sequencing libraries were prepared as described in Baym et al. (*50*). Sequencing was performed using a NextSeq instrument, producing 75 bp, paired-end reads. Resulting data was aligned to the *E. coli* C321.delA non-auxotrophic but recoded reference sequence (Genbank CP006698.1) and the sequence of the plasmid encoding nsAA incorporation machinery. The Millstone software suite was used to identify variants, provide measures of sequencing confidence, and predict their likelihood of altering gene function (*51*). Genomic variants of low confidence, low sequence coverage, or presence in the ancestral strain were discarded, prioritizing variants observed in three non-essential genes that encode membrane proteins: *acrB*. *emrD*, and *trkH*.

Subsequent genomic sequencing was performed on genomic DNA extracted from the evolved populations and ancestral clone using the DNeasy Blood and Tissue Kit (Qiagen). Genomic DNA was then sent to the Microbial Genome Sequencing Center (MiGS) in Pittsburgh, PA. Variants were identified through the variant calling service from MiGS.

Allelic reconstruction

Multiplex Automatable Genomic Engineering (MAGE) (*52*) was used to inactivate the endogenous *mutS* gene in the DEP strain. Overnight cultures were diluted 100-fold into 3 mL LB containing chloramphenicol, BipA, L-arabinose, and Tris HCl buffer and grown at 34 °C until mid-log. The genome-integrated lambda Red cassette in this C321.ΔA-derived strain was induced in a shaking water bath (42 °C, 300 rpm, 15 minutes), followed by cooling the culture tube on ice for at least two minutes. The cells were made electrocompetent at 4°C by pelleting 1 mL of culture (8,000 rcf, 30 seconds) and washing thrice with 1 mL ice-cold 10% glycerol. Electrocompetent pellets were resuspended in 50μL of dH_2O containing the desired DNA, for MAGE oligonucleotides, 5 μM of each oligonucleotide was used. Allele-specific colony PCR was used to

identify desired colonies resulting from MAGE as previously described (*53*). Oligonucleotides used for MAGE and for allele-specific colony PCR are included in **Table S4**.

Investigation of media conditions on reconstructed alleles

This assay was performed using a similar protocol as described in the *Measurement of doubling times* section. The cultures for DEP and its single mutants were grown overnight in 100 μM BipA. Then cultures were diluted 100X in the media specified. Those conditions include standard media conditions as well as single component changes: 0% SDS, 0.01% SDS, 0.02% (wt/v) Arabinose, 0 mM Tris-HCl, 30 μg/mL Chloramphenicol. The cultures were grown in triplicate for each condition and in a SpectraMax i3 plate reader, shaking at 34 °C for 24 h. The OD_{600} was measured about every 5 mins. The doubling times were then calculated as previously described.

Bacterial and mammalian co-culturing

HEK293T cells containing one copy of mCherry marker (red) integrated into the AAVS1 locus, were grown at 40-50% confluency in DMEM high glucose medium (Thermo Fisher cat# 11965175) with 10% inactivated Fetal Bovine Serum (FBS Thermo Fisher cat# 10082147), 100X MEM NEAA (non-essential amino acids Thermo Fisher cat# 11140050), and 100X diluted anti-anti cocktail (Antibiotic-Antimycotic - 10,000 units/mL of penicillin, 10,000 μg/mL of streptomycin, and 25 μg/mL of Gibco Amphotericin B - Thermo Fisher cat# 15240112). Commercially acquired *E. coli* DH5α bacteria were used as control to the *E. coli* DEP *mutS*¯ or DEP* strain. A plasmid containing Clover (green marker) containing a UAA stop codon compatible with the biocontained strain DEP, and under the selection marker ampicillin was transformed into both DH5α and DEP* strains in order to visualize them with the mammalian cells (red). BipA-dependent auxotroph DEP* bacteria were grown to OD 0.6, in LB medium supplemented with 1% L-arabinose, 100 μM BipA, 100 ug/ml carbenicillin and 25ug/ml chloramphenicol and then washed 3 times with 1X PBS. DEP* culture conditions with L-arabinose, carbenicillin, and chloramphenicol supplements did slightly affect HEK293T early cell growth compared to untreated cells, though insufficient to affect conclusions drawn from these experiments. DH5α strain was grown to OD 0.6 with 100ug/ml carbenicillin. The pellet of 10-milliliter bacterial cell culture was re-suspended in mammalian cell medium as described above without any antibiotics and anti-anti, and split equally among all conditions and their replicates. Auxotroph bacteria are added to HEK293T cells plated in pre-treated 12-well plates in 2 ml mammalian cell medium. The co-culture is incubated overnight before media with bacterial cells is removed and HEK293T cells are washed three times with 1X PBS (phosphate buffered saline Thermo Fisher cat# 10010023) and replenished with fresh media as conditions indicate. Media was replaced and added fresh to all conditions daily for 7 days. Imaging cells was done with the inverted microscope Nikon Eclipse TS100 at Day 2, Day 4, and Day 7 post initial co-culture at 200X magnification.

Conditions:

Control: HEK293T grown in regular 10% FBS media with anti-anti and NEAA as described above.

DH5α: HEK293T cells co-cultured with this strain in mammalian cell media supplemented with 100ug/ml carbenicillin to maintain plasmid during growth, and absence of anti-anti.

DH5α; anti-anti (antibiotic cocktail): HEK 293T cells co-cultured with this strain in mammalian cell media supplemented with 100ug/ml carbenicillin to maintain plasmid during growth, and presence of anti-anti cocktail.

DH5α; anti-anti after Day 2: HEK 293T cells co-cultured with this strain in mammalian cell media supplemented with 100ug/ml carbenicillin to maintain plasmid during growth, and absence of anti-anti cocktail. At 48 hours anti-anti added and maintained to Day 7.

DH5α; anti-anti; no anti-anti after Day 2: HEK 293T cells co-cultured with this strain in mammalian cell media supplemented with 100ug/ml carbenicillin to maintain plasmid during growth, and presence of anti-anti until Day 2. After Day 2 no anti-anti added and maintained to Day 7.

DEP*: HEK 293T cells co-cultured with the biocontained strain in media supplemented with L-arabinose, 25ug/ml chloramphenicol and 100ug/ml carbenicillin to maintain bacteria and green marker. No bipA or anti-anti added.

DEP*; bipA: HEK 293T cells co-cultured with the biocontained strain in media supplemented with L-arabinose, 25ug/ml chloramphenicol and 100ug/ml carbenicillin to maintain bacteria and green marker. 100 uM bipA and no anti-anti added.

DEP*; bipA after Day 2: HEK 293T cells co-cultured with the biocontained strain in media supplemented with L-arabinose, 25ug/ml chloramphenicol and 100ug/ml carbenicillin to maintain bacteria and green marker. No bipA or anti-anti added. At 48 hours bipA at 100uM concentration added and maintained to Day 7.

DEP*; anti-anti: HEK 293T cells co-cultured with the biocontained strain in media supplemented with anti-anti, L-arabinose, 25ug/ml chloramphenicol and 100ug/ml carbenicillin to maintain bacteria and green marker. No bipA added.

DEP*; bipA; anti-anti: HEK 293T cells co-cultured with the biocontained strain in media supplemented with anti-anti, L-arabinose, 25ug/ml chloramphenicol and 100ug/ml carbenicillin to maintain bacteria and green marker. 100uM bipA added.

Persistence

Persistence was evaluated by two kinds of assays: Plate reader and colony count. For the plate reader case, DEP, DEP.e3, DEP.e4, and DEP.e5 cultures were grown overnight in permissible media conditions with 100 μM BipA. For cells harvested at mid-exponential phase, the cultures were diluted 100X and grown to that state. Both stationary phase and mid-exponential phase cultures were then washed twice with LB media and resuspended in the original volume of non-permissible media containing all specified media components except BipA. The resuspended cultures were then diluted 100X into non-permissible media in triplicate for each time point to be tested. The specified concentration of BipA was then added back to those cultures at the specified time points. Typically, the BipA re-addition occurred at 10 μM or 5 μM concentrations and at hourly or daily intervals. The cultures were then incubated with shaking in SpectraMax i3 plate readers in a flat, clear bottom 96-well plate with breathable and optically transparent seal for an upwards of 84 hours at 34 °C. Approximately every five minutes the OD_{600} was measured to determine cell growth kinetics.

Data Repository

Data files including the .stl file for the custom chemostat sleeve, raw sequencing reads, and variant calling analysis for the evolved strains are deposited in the Kunjapur Lab Github: https://github.com/KunjapurLab/evolved_synthetic_auxotrophs

397

398

399

References and Notes:

1. M. T. Parker, A. M. Kunjapur, Deployment of Engineered Microbes: Contributions to the Bioeconomy and Considerations for Biosecurity. *Heal. Secur.* **18**, 278–296 (2020).
2. J. R. Bober, C. L. Beisel, N. U. Nair, Synthetic Biology Approaches to Engineer Probiotics and Members of the Human Microbiota for Biomedical Applications. *Annu. Rev. Biomed. Eng.* **20**, 277–300 (2018).
3. T. Ozdemir, A. J. H. Fedorec, T. Danino, C. P. Barnes, Synthetic Biology and Engineered Live Biotherapeutics: Toward Increasing System Complexity. *Cell Syst.* **7** (2018), pp. 5–16.
4. M. R. Charbonneau, V. M. Isabella, N. Li, C. B. Kurtz, Developing a new class of engineered live bacterial therapeutics to treat human diseases. *Nat. Commun.* **11**, 1738 (2020).
5. G. A. Bacon, T. W. Burrows, M. Yates, The effects of biochemical mutation on the virulence of Bacterium typhosum; the loss of virulence of certain mutants. *Br. J. Exp. Pathol.* **32**, 85–96 (1951).
6. S. K. Hoiseth, B. A. D. Stocker, Aromatic-dependent Salmonella typhimurium are non-virulent and effective as live vaccines. *Nature*. **291**, 238–239 (1981).
7. R. J. Thompson, H. G. Bouwer, D. A. Portnoy, F. R. Frankel, Pathogenicity and immunogenicity of a Listeria monocytogenes strain that requires D-alanine for growth. *Infect. Immun.* **66**, 3552–61 (1998).
8. D. A. Smith, T. Parish, N. G. Stoker, G. J. Bancroft, Characterization of auxotrophic mutants of Mycobacterium tuberculosis and their potential as vaccine candidates. *Infect. Immun.* **69**, 1142–1150 (2001).
9. J. Hinchey *et al.*, Lysine auxotrophy combined with deletion of the secA2 gene results in a safe and highly immunogenic candidate live attenuated vaccine for tuberculosis. *PLoS One*. **6** (2011), doi:10.1371/journal.pone.0015857.
10. M. P. Cabral *et al.*, Design of live attenuated bacterial vaccines based on D-glutamate auxotrophy. *Nat. Commun.* **8**, 15480 (2017).
11. J. Tjuvajev *et al.*, in *Journal of Controlled Release* (Elsevier, 2001), vol. 74, pp. 313–315.
12. L. Steidler *et al.*, Biological containment of genetically modified Lactococcus lactis for intestinal delivery of human interleukin 10. *Nat. Biotechnol.* **21**, 785–789 (2003).

13. M. Zhao *et al.*, Tumor-targeting bacterial therapy with amino acid auxotrophs of GFP-expressing Salmonella typhimurium. *Proc. Natl. Acad. Sci. U. S. A.* **102**, 755–760 (2005).
14. H. Braat *et al.*, A Phase I Trial With Transgenic Bacteria Expressing Interleukin-10 in Crohn's Disease. *Clin. Gastroenterol. Hepatol.* **4**, 754–759 (2006).
15. D. S. Leventhal *et al.*, Immunotherapy with engineered bacteria by targeting the STING pathway for anti-tumor immunity. *Nat. Commun.* **11**, 2739 (2020).
16. S. B. Formal, L. S. Baron, W. Spilman, Studies on the virulence of a naturally occurring mutant of Salmonella typhosa. *J. Bacteriol.* **68**, 117 (1954).
17. M. D. L. G. Curcho, Mutation to Tryptophan Independence in Eberthella typhosa. *J. Bacteriol.* **56**, 374 (1948).
18. P. Fildes, K. Whitaker, "Training" or Mutation of Bacteria. *Br. J. Exp. Pathol.* **29**, 240 (1948).
19. S. C. Liu, N. P. Minton, A. J. Giaccia, J. M. Brown, Anticancer efficacy of systemically delivered anaerobic bacteria as gene therapy vectors targeting tumor hypoxia/necrosis. *Gene Ther.* **9**, 291–296 (2002).
20. J. C. Anderson, E. J. Clarke, A. P. Arkin, C. A. Voigt, Environmentally controlled invasion of cancer cells by engineered bacteria. *J. Mol. Biol.* **355**, 619–627 (2006).
21. S. Pande *et al.*, Metabolic cross-feeding via intercellular nanotubes among bacteria. *Nat. Commun.* **6**, 6238 (2015).
22. K. Zengler, L. S. Zaramela, The social network of microorganisms - How auxotrophies shape complex communities. *Nat. Rev. Microbiol.* **16** (2018), pp. 383–390.
23. D. J. Mandell *et al.*, Biocontainment of genetically modified organisms by synthetic protein design. *Nature*. **518**, 55–60 (2015).
24. A. J. Rovner *et al.*, Recoded organisms engineered to depend on synthetic amino acids. *Nature*. **518**, 89–93 (2015).
25. T. M. Wannier *et al.*, Adaptive evolution of genomically recoded Escherichia coli. *Proc. Natl. Acad. Sci. U. S. A.* **115** (2018), doi:10.1073/pnas.1715530115.
26. B. G. Wong, C. P. Mancuso, S. Kiriakov, C. J. Bashor, A. S. Khalil, Precise, automated control of conditions for high-throughput growth of yeast and bacteria with eVOLVER. *Nat. Biotechnol.* **36**, 614–623 (2018).
27. E. Toprak *et al.*, Building a morbidostat: an automated continuous-culture device for

studying bacterial drug resistance under dynamically sustained drug inhibition. *Nat. Protoc.* **8**, 555–67 (2013).

28. K. Nishino, A. Yamaguchi, Analysis of a complete library of putative drug transporter genes in Escherichia coli. *J. Bacteriol.* **183**, 5803–5812 (2001).

29. E. J. Levin, M. Zhou, Recent progress on the structure and function of the TrkH/KtrB ion channel. *Curr. Opin. Struct. Biol.* **27** (2014), pp. 95–101.

30. L. M. Dedkova, N. E. Fahmi, S. Y. Golovine, S. M. Hecht, Construction of modified ribosomes for incorporation of D-amino acids into proteins. *Biochemistry*. **45**, 15541–15551 (2006).

31. R. Maini *et al.*, Protein Synthesis with Ribosomes Selected for the Incorporation of β-Amino Acids. *Biochemistry*. **54**, 3694–3706 (2015).

32. M. Ettayebi, S. M. Prasad, E. A. Morgan, Chloramphenicol-erythromycin resistance mutations in a 23S rRNA gene of Escherichia coli. *J. Bacteriol.* **162**, 551–557 (1985).

33. H. H. Wang *et al.*, Programming cells by multiplex genome engineering and accelerated evolution. *Nature*. **460**, 894–898 (2009).

34. L. Goers, P. Freemont, K. M. Polizzi, Co-culture systems and technologies: taking synthetic biology to the next level. *J R Soc Interface*. **11** (2014), doi:10.1098/rsif.2014.0065.

35. T. L. A. Nguyen, S. Vieira-Silva, A. Liston, J. Raes, How informative is the mouse for human gut microbiota research? *DMM Dis. Model. Mech.* **8**, 1–16 (2015).

36. W. Paul, C. Marta, V. de W. Tom, Resolving host–microbe interactions in the gut: the promise of in vitro models to complement in vivo research. *Curr. Opin. Microbiol.* **44** (2018), pp. 28–33.

37. K. M. Mason, N. J. Bigley, P. S. Fink, Development of a novel in vitro co-culture system for studying host response to native bacterial antigens. *J. Immunol. Methods*. **211**, 147–158 (1998).

38. A. Parlesak, D. Haller, S. Brinz, A. Baeuerlein, C. Bode, Modulation of Cytokine Release by Differentiated CACO-2 Cells in a Compartmentalized Coculture Model with Mononuclear Leucocytes and Nonpathogenic Bacteria. *Scand. J. Immunol.* **60**, 477–485 (2004).

39. M. H. M. C. Nuenen *et al.*, The influence of microbial metabolites on human intestinal

epithelial cells and macrophages in vitro. *FEMS Immunol. Med. Microbiol.* **45**, 183–189 (2005).

40. G. Noel *et al.*, A primary human macrophage-enteroid co-culture model to investigate mucosal gut physiology and host-pathogen interactions. *Sci. Rep.* **7**, 1–14 (2017).

41. K. Höner zu Bentrup *et al.*, Three-dimensional organotypic models of human colonic epithelium to study the early stages of enteric salmonellosis. *Microbes Infect.* **8**, 1813–1825 (2006).

42. J. Kim, M. Hegde, A. Jayaraman, Co-culture of epithelial cells and bacteria for investigating host-pathogen interactions. *Lab Chip*. **10**, 43–50 (2010).

43. H. J. Kim, D. Huh, G. Hamilton, D. E. Ingber, Human gut-on-a-chip inhabited by microbial flora that experiences intestinal peristalsis-like motions and flow. *Lab Chip*. **12**, 2165–2174 (2012).

44. H. J. Kim, H. Li, J. J. Collins, D. E. Ingber, Contributions of microbiome and mechanical deformation to intestinal bacterial overgrowth and inflammation in a human gut-on-a-chip. *Proc. Natl. Acad. Sci. U. S. A.* **113**, E7–E15 (2016).

45. P. Shah *et al.*, A microfluidics-based in vitro model of the gastrointestinal human-microbe interface. *Nat. Commun.* **7**, 11535 (2016).

46. A. M. Kunjapur *et al.*, Engineering posttranslational proofreading to discriminate nonstandard amino acids. *Proc. Natl. Acad. Sci. U. S. A.* **115**, 619–624 (2018).

47. M. G. Napolitano, Morbidostat code, (available at https://github.com/mnapolitano89/morbidostat_control).

48. T. M. Wannier *et al.*, Adaptive evolution of genomically recoded Escherichia coli. *Proc. Natl. Acad. Sci. U. S. A.* **115**, 3090–3095 (2018).

49. D. J. Mandell *et al.*, Biocontainment of genetically modified organisms by synthetic protein design. *Nature*. **518**, 55–60 (2015).

50. M. Baym *et al.*, Inexpensive Multiplexed Library Preparation for Megabase-Sized Genomes. *PLoS One*. **10**, e0128036 (2015).

51. D. B. Goodman *et al.*, Millstone: software for multiplex microbial genome analysis and engineering. *Genome Biol.* **18**, 101 (2017).

52. H. H. Wang *et al.*, Programming cells by multiplex genome engineering and accelerated evolution. *Nature*. **460**, 894–898 (2009).

53. F. J. Isaacs *et al.*, Precise manipulation of chromosomes in vivo enables genome-wide codon replacement. *Science (80-.).* **333**, 348–353 (2011).
54. H. Okusu, D. Ma, H. Nikaido, AcrAB Efflux Pump Plays a Major Role in the Antibiotic Resistance Phenotype of Escherichia coli Multiple-Antibiotic-Resistance (Mar) Mutants. *J Bacteriol*. **178**, 306–308 (1996).
55. D. Ma *et al.*, Genes acrA and acrB encode a stress-induced efflux system of Escherichia coli. *Mol. Microbiol.* **16**, 45–55 (1995).
56. E. B. Tikhonova, Y. Yamada, H. I. Zgurskaya, Sequential mechanism of assembly of multidrug efflux pump AcrAB-TolC. *Chem. Biol.* **18**, 454–463 (2011).
57. E. C. A. Goodall *et al.*, The essential genome of Escherichia coli K-12. *MBio*. **9** (2018), doi:10.1128/mBio.02096-17.
58. R. Nakashima, K. Sakurai, S. Yamasaki, K. Nishino, A. Yamaguchi, Structures of the multidrug exporter AcrB reveal a proximal multisite drug-binding pocket. *Nature* (2011), doi:10.1038/nature10641.
59. T. Eicher *et al.*, Transport of drugs by the multidrug transporter AcrB involves an access and a deep binding pocket that are separated by a switch-loop. *Proc. Natl. Acad. Sci. U. S. A.* **109**, 5687–5692 (2012).
60. M. Zwama *et al.*, Multiple entry pathways within the efflux transporter AcrB contribute to multidrug recognition. *Nat. Commun.* **9**, 124 (2018).
61. R. T. Müller *et al.*, Switch Loop Flexibility Affects Substrate Transport of the AcrB Efflux Pump. *J. Mol. Biol.* **429**, 3863–3874 (2017).
62. T. Xianwei, L. Diannan, W. Boxiong, Substrate transport pathway inside outward open conformation of EmrD: a molecular dynamics simulation study. *Mol. BioSyst*. **12**, 2634 (2016).
63. K. Koita, C. V. Rao, Identification and Analysis of the Putative Pentose Sugar Efflux Transporters in Escherichia coli. *PLoS One*. **7**, e43700 (2012).
64. R. M. Morgan-Kiss, C. Wadler, J. E. Cronan, Long-term and homogeneous regulation of the Escherichia coli araBAD promoter by use of a lactose transporter of relaxed specificity. *Proc. Natl. Acad. Sci. U. S. A.* **99**, 7373–7377 (2002).
65. A. Khlebnikov, Risa, T. Skaug, T. A. Carrier, J. D. Keasling, Regulatable arabinose-inducible gene expression system with consistent control in all cells of a culture. *J.*

Bacteriol. **182**, 7029–7034 (2000).

66. Y. Yin, X. He, P. Szewczyk, T. Nguyen, G. Chang, Structure of the Multidrug Transporter EmrD from Escherichia coli. *Science (80-.).* **312**, 741–744 (2006).

67. H. Zhang *et al.*, TrkA undergoes a tetramer-to-dimer conversion to open TrkH which enables changes in membrane potential. *Nat. Commun.* **11**, 1–11 (2020).

Acknowledgements:

We thank Caleb Bashor for assistance setting up the continuous evolution platform, and Sabyasachi Sen and Neil Butler for manuscript comments. We thank Timothy Wannier for sharing the Clover plasmid, and Ellen Schrock for helping generate the mCherry stable HEK293T cell line. **Funding:** This work was primarily funded by grants to GMC from the U.S. Dept. of Energy (FG02-02ER63445) and the FunGCAT program from the Office of the Director of National Intelligence (ODNI), Intelligence Advanced Research Projects Activity (IARPA), via the Army Research Office (ARO) under Federal Award No. W911NF-17-2-0089. We also acknowledge support from the National Institute of General Medical Sciences of the National Institutes of Health under a Chemistry-Biology Interface Training Grant that supported MAJ (Award Number T32GM133395), and a grant to AMK from the National Science Foundation (MCB2027092).
Author Contributions: AMK: Conceptualization, Investigation, Writing, Supervision, Funding acquisition **MGN:** Conceptualization, Methodology, Software, Investigation, Writing **EH:** Conceptualization, Methodology, Investigation, Writing **KN:** Investigation **EMA:** Supervision, Funding acquisition **MGS/MAJ/SI:** Investigation **DJM:** Conceptualization, Methodology **GMC:** Supervision, Funding acquisition. **Competing Interests:** The authors declare the following competing financial interest(s): GMC has related financial interests in 64-x, EnEvolv, and GRO Biosciences. For a complete list of GMC's financial interests, please visit arep.med.harvard.edu/gmc/tech.html. DJM is an employee of and equity holder in GRO Biosciences. Harvard College has an issued patent covering the DEP strain. **Data and materials availability:** The DEP strain and evolved clonal isolates are restricted for distribution to academics for research use only. These four strains will be available on the Addgene Plasmid Repository (ID 171711-171714). Requests from for-profits to access the material will be sent to Harvard to take a license before receiving the strain. All data is available in the manuscript or the supplementary materials.

List of Supplementary Materials

Figures S1-S14

Tables S1-S4

Figure Captions

Figure 1. Design and operation of custom chemostats for automated continuous evolution. (A) Illustration of a smart sleeve connected to separate non-permissive media and biphenylalanine (BipA, structure shown in blue) feed lines for automated adjustment of BipA concentration based on growth rate. Pumps and optics are integrated with Arduino controller hardware and Python software based on the eVOLVER do-it-yourself automated culturing framework. (B) Working algorithm for maintenance of cultures in continuous evolution mode. Criteria for lowering the BipA concentration is based on the difference in time elapsing between OD peaks (Δt_{peak} OD). Smaller time elapsed between OD peaks is indicative of higher growth rates, triggering decrease of BipA concentration when below a threshold value. (C) Representative configuration of hardware for parallelized evolution in triplicate, with three empty sleeves shown. Photo Credit: Michael Napolitano, Harvard Medical School.

Figure 2. Continuous evolution of synthetic auxotrophs leads to adaptation to lower BipA concentration rather than escape. (A) Timeline for continuous evolution, with detection limits for escape frequency assays shown in parentheses. (B) Doubling times of progenitor and evolved synthetic auxotrophs as a function of BipA concentration, normalized to the doubling time of DEP at 100 μM BipA. Error bars represent the standard deviation across technical triplicates within the same experiment.

Figure 3. Whole genome sequencing and reconstruction of alleles shared across populations of evolved synthetic auxotrophs. (A) List of alleles identified through next-generation sequencing. †Sequencing results originally obtained during the project identified this EmrD allele as a 33 bp deletion, which was then reconstructed in the experiment shown in panel B. However, resequencing performed at the end of the project identified the allele as a 39 bp deletion and was confirmed by Sanger sequencing. A repetitive GGCGCG nucleotide sequence corresponding to G323-A324 and G336-A337 creates ambiguity about the precise positional numbering of the deletion. However, the 3 possible 13 AA deletions (323-335, 324-336, 325-337) result in the same final protein sequence. (B) Effect of reconstructed allele in DEP progenitor on doubling time as a

function of BipA concentration, normalized to the doubling time of DEP at 100 μM BipA. Error bars represent the standard deviation across technical triplicates within the same experiment.

Figure 4. Imaging of bacterial-mammalian co-cultures. Bacteria were added to HEK293T cell cultures and co-incubated for 24 hours before washing and replenishing media. HEK293T cells express mCherry, whereas bacterial cells express Clover green protein marker. Images were taken at Days 2, 4, and 7 after co-incubation. (A) Untreated HEK293T cells. (B) HEK293T with commercial E. coli DH5α in the absence of antibiotic cocktail. (C) HEK293T with DH5α in presence of antibiotic cocktail. (D) HEK293T and DEP* (mismatch repair inactivated to create hypermutator phenotype) in the absence of BipA. (E) HEK293T cells and DEP* in the presence of BipA. (F) HEK293T and DEP* in the absence of BipA until Day 2 (identical at this point to condition in Panel D), and then 100 μM of BipA added to this condition daily until Day 7.

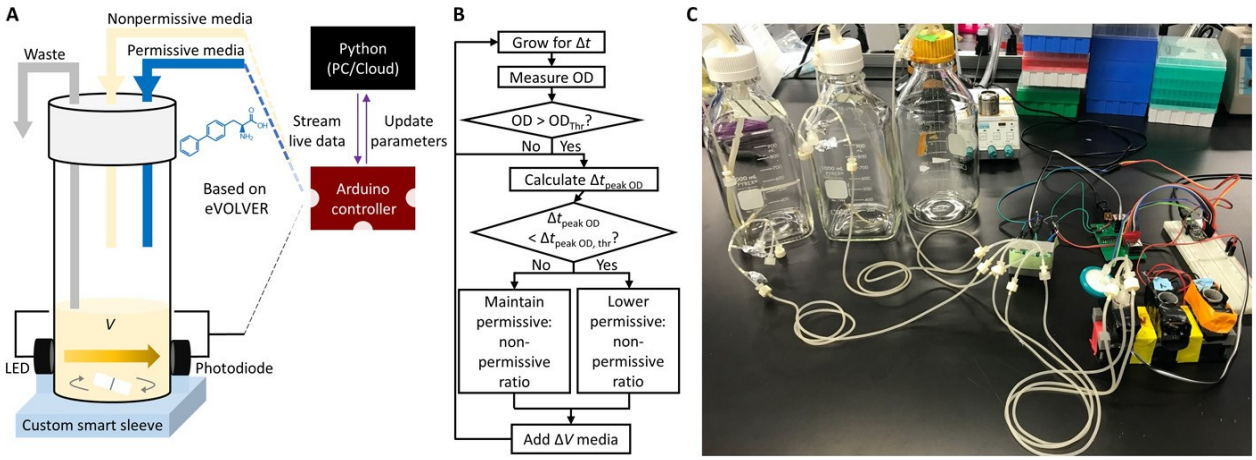
A
Nonpermissive media
Waste
Permissive media
Python
(PC/Cloud)
Stream
live data
Update
parameters
Arduino
controller
Based on
eVOLVER
V
LED
Photodiode
Custom smart sleeve
B
Grow for Δt
Measure OD
OD > OD_Thr?
No
Yes
Calculate Δt_peak OD
Δt_peak OD
< Δt_peak OD, thr?
No
Yes
Maintain
permissive:
non-
permissive
ratio
Lower
permissive:
non-
permissive
ratio
Add ΔV media
C

Figure 1.

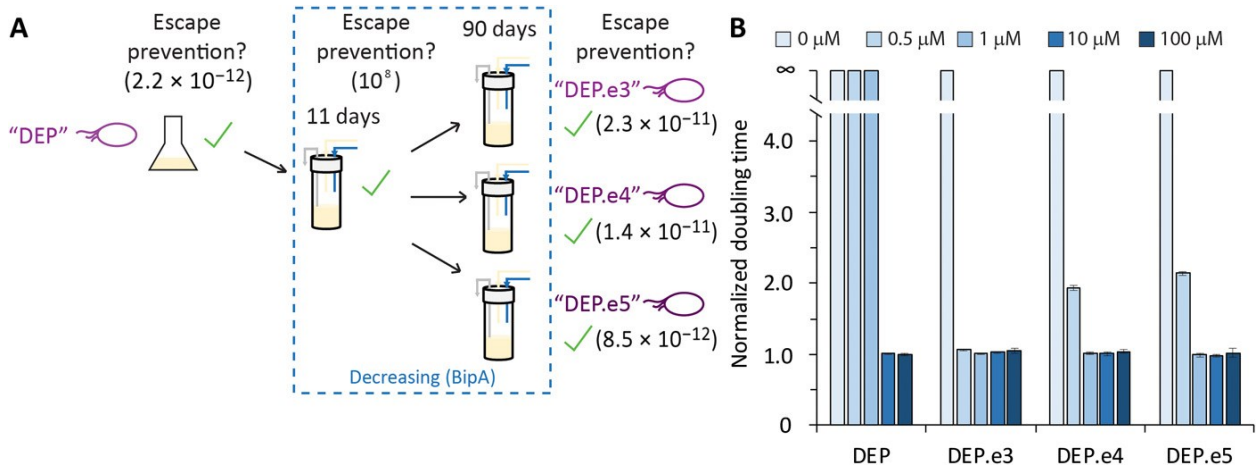

638

639 **Figure 2.**

640

A

Variant	DEP.e3	DEP.e4	DEP.e5
AcrB_G619E	✓	✓	✓
EmrD_G314R	✓		
EmrD(G323_A335del)†		✓	✓
TrkH_I143S	✓	✓	✓

B

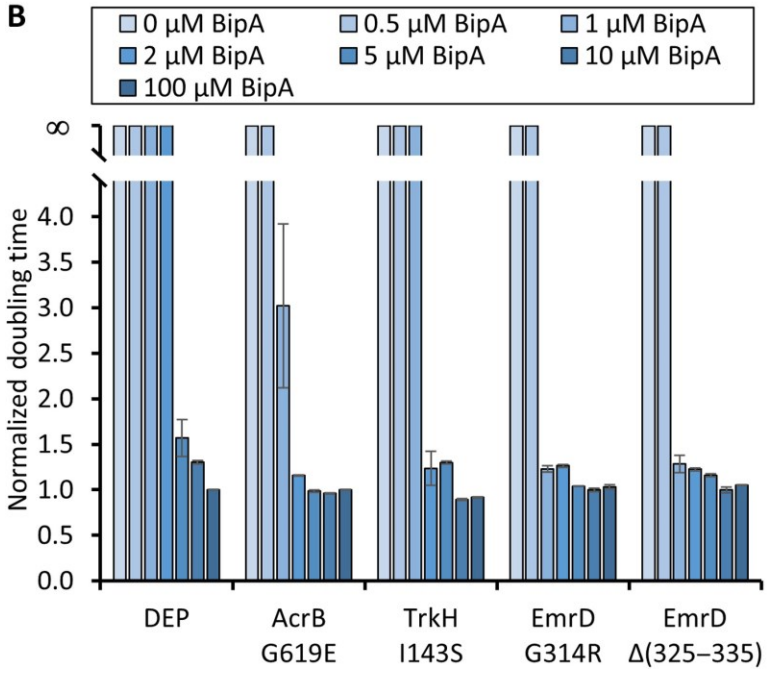

Figure 3.

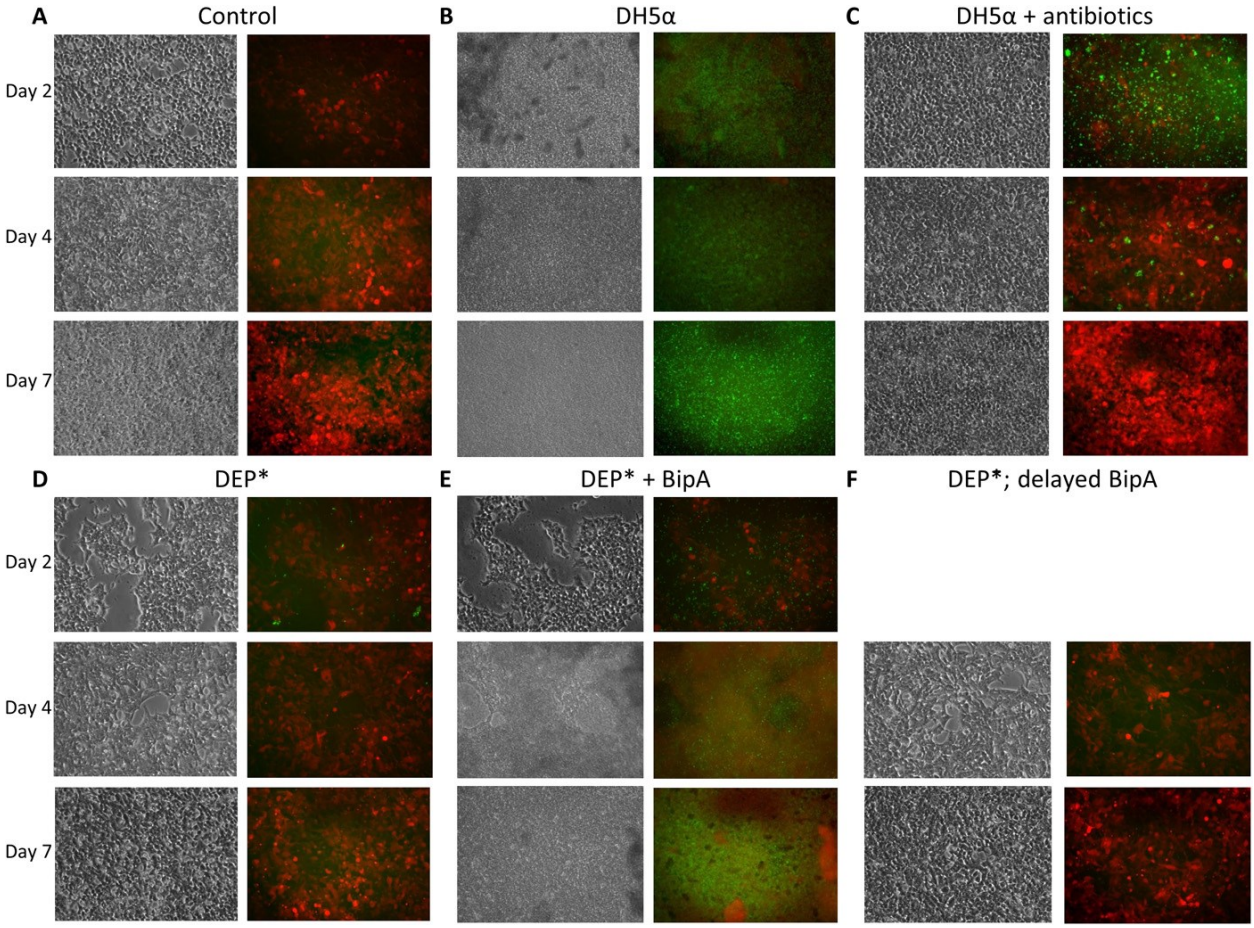

644

645 **Figure 4.**